Performance predictions for a laser-intensified thermal beam for use in high-resolution focused-ion-beam instruments

S. H. W. Wouters, G. ten Haaf, R. P. M. J. W. Notermans,[*] N. Debernardi,[†] P. H. A. Mutsaers, O. J. Luiten, and E. J. D. Vredenbregt[‡]

Department of Applied Physics, Eindhoven University of Technology, P.O. Box 513, 5600 MB Eindhoven, Netherlands

(Received 17 October 2014; published 15 December 2014)

Photoionization of a laser-cooled and compressed atomic beam from a high-flux thermal source can be used to create a high-brightness ion beam for use in focused-ion-beam instruments. Here we show using calculations and Doppler cooling simulations that an atomic rubidium beam with an equivalent brightness of 2.1×10^7 A/(m^2 sr eV) can be created using a compact 5 cm long two-dimensional magneto-optical compressor. If this can be conserved during the photoionization process, this leads to an ion beam brightness an order of magnitude higher than produced by a liquid metal ion source. The source is also capable of producing a flux of 6.2×10^9 s^{-1} that results in a substantial beam current of 1 nA once fully ionized.

DOI: 10.1103/PhysRevA.90.063817 PACS number(s): 37.20.+j, 37.10.De, 41.75.Ak, 89.20.Bb

I. INTRODUCTION

The focused ion beam (FIB) is a valuable tool in the semiconductor industry since it enables imaging and modification of structures on the nanometer size scale [1]. The most important property of a FIB, the spot size versus current curve, is largely determined by the transverse reduced brightness (hereafter abbreviated as the brightness) and longitudinal energy spread of its ion source. The current state of the art for modification of structures is the liquid metal ion source (LMIS), which creates a gallium ion beam with a brightness of 10^6 A/(m^2 sr eV) and a longitudinal energy spread of 4.5 eV [2,3]. Note that the gas field ionization source (GFIS) is a promising alternative for ion beam imaging with a brightness of more than 10^9 A/(m^2 sr eV) [4] and a longitudinal energy spread of less than 1 eV [4], allowing subnanometer resolution. Due to the lower sputter yield and subsurface damage of the helium [4] and neon [5] based GFISs, this apparatus is less suitable for sample modification than the LMIS [6]. In order to create a FIB with the possibility of high-resolution sample manipulation, a heavy-ion based source is required with a smaller longitudinal energy spread than the LMIS and at least equal brightness. Furthermore, currents up to 1 nA should be possible and a compact source is preferred.

Several research groups are working on reaching these goals. The nano-aperture ion source [7] for example aims at creating an ion beam by electron impact ionization of a high-density gas. A different idea is to use laser-cooled atoms as a source for cold ions as was proposed by Freinkman *et al.* [8]. Apart from promising high-brightness ion beams, laser cooling can be applied to a variety of atomic species ranging from the alkali and alkaline metals, several transition and rare-earth metals, and some *p*-block materials, which would open up new possibilities for FIB users. The ultracold ion source (UCIS) [9] and magneto-optical trap ion source (MOTIS) [10] both use laser cooling and trapping in three dimensions followed by in-field photoionization to create ion bunches or beams. Although longitudinal energy spreads down to 20 meV have been demonstrated [11], the target brightness could not be achieved with these sources [12]. This is because refilling the ionization region in the MOT is slow due to the low diffusion rate caused by the small velocity of the atoms. To circumvent this problem one could increase the loading rate by addition of a two-dimensional (2D) MOT or low-velocity intense source (LVIS) [13] to the system. Omitting the 3D MOT completely is a more direct way of reaching the same goal. Knuffman *et al.* [14] have reported on a FIB based on a vapor cell 2D+ MOT combined with two-step photoionization with an inferred brightness of 10^7 A/(m^2 sr eV) at a current of several picoamperes. Cooling and compressing atoms originating from a thermal source (such as a Knudsen cell) allows for the creation of beams with equal brightness but even higher currents since the availability of the very large flux from such a source allows the selection of the best part of the laser-cooled atom beam, thus keeping high brightness up to currents of the target 1 nA. The FIB source considered here, as the one of Kime *et al.* [15], therefore uses a Knudsen cell as the atomic source. In our case, the Knudsen cell is connected to a heated collimation tube [16,17] which increases the lifetime of the atomic reservoir by more than an order of magnitude and alters the velocity distribution such that even more atoms can be captured in the magneto-optical compressor (MOC).

Figure 1 shows a schematic representation of the proposed source. The atomic beam is formed from a Knudsen cell with an aperture radius r connected to a collimating tube with equal radius r and length L_s. After leaving the tube, the atoms are introduced into a magneto-optical compressor with length L_c which cools the atoms in the transverse direction to a mK temperature and compresses it to a beam with a radius r_f. Immediately after leaving the compressor, the atoms are photoionized in a two-step process by two crossed laser beams. At the intersection of these beams, ions are formed which are accelerated by the electric field E between two accelerator

[*]Present address: LaserLaB, Department of Physics and Astronomy, VU University Amsterdam, De Boelelaan 1081, 1081 HV Amsterdam, Netherlands.

[†]Present address: Equipment for Additive Manufacturing, Netherlands Organization for Applied Scientific Research TNO, De Rondom 1, 5612 AP Eindhoven, Netherlands.

[‡]Corresponding author: e.j.d.vredenbregt@tue.nl

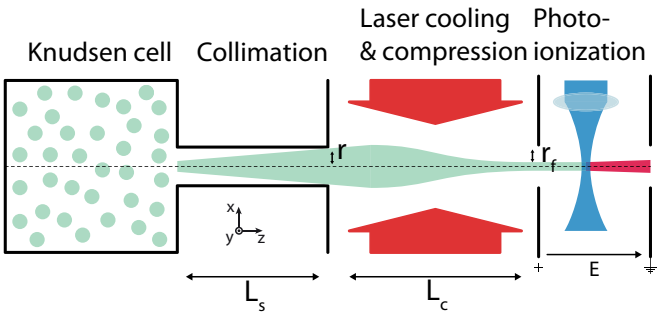

FIG. 1. (Color online) Schematic drawing of an atomic beam laser-cooled ion source in the xz plane. From the left to the right, an atomic beam is formed from a Knudsen cell connected to a collimating tube with a radius r and length L_s. These atoms are then laser-cooled and compressed over a distance L_c to a final radius of r_f. At the right the atomic beam is photoionized in an electric field E to create the ion beam.

plates. The resulting ions are focused by an (electrostatic) focusing column.

This design can be used for a broad range of atomic species (except for the metastable ones) although the detailed design of the Knudsen cell and collimating tube will look different for elements with a high melting point. As a specific example, rubidium will be used which has a rich history in laser cooling and is, due to its higher mass, expected to be more effective for ion beam milling than gallium. All relevant constants for the two stable isotopes of rubidium are given in Table I.

This paper discusses calculations and simulations of the proposed source that show that the desired equivalent atomic beam brightness and current can be achieved using realistic parameters for the atomic source and the MOC. In Sec. II an analytical model is set up to predict the performance of the system. Section III discusses Doppler cooling simulations of the MOC in regimes where the analytical model does not hold. Section IV briefly describes which steps need to be taken to make use of the high atomic beam brightness in an actual FIB. Finally, Sec. V presents the conclusions of this work.

TABLE I. Atomic constants used in the calculations and the simulations. All data is taken from [18] except when indicated otherwise. Note that the values for p^* and T^* are only valid for temperatures between 312 and 550 K.

Parameter (unit)	Symbol	^{85}Rb	^{87}Rb
Abundance (%)	ab	72.2	27.8
Mass (amu)	m	84.91	86.91
Nuclear spin quantum number (−)	I	5/2	3/2
Pressure constant (10^9 Pa)	p^*	2.05	2.05
Temperature constant (10^3 K)	T^*	9.30	9.30
van der Waals radius [19] (pm)	r_{vdw}	303	303
Natural linewidth (MHz)	$\Gamma/2\pi$	6.07	6.07
Cooling wavelength (nm)	λ	780	780
Saturation intensity (W/m^2)	I_{sat}	16.7	16.7
Doppler temperature limit (μK)	T_D	146	146
Ionization wavelength[a] (nm)	λ_i	480	480
Ionization cross section[a] [20] (10^{-21} m^2)	σ_i	1.48	1.48

[a]From $5^2P_{3/2}$ excited state.

II. ANALYTICAL MODEL

An analytical model is set up based on standard theoretical treatment of laser cooling as formulated by Metcalf and van der Straten [21] to give a understanding of the relevant parameters of the source and to verify Doppler cooling simulations in the regime where the theoretical predictions of laser cooling are valid. In short, the brightness is calculated of a skimmed thermal beam from a Knudsen cell that is cooled to the Doppler temperature and compressed to such a radius that the kinetic energy of the atoms equals their spring energy. The actual atomic structure of rubidium is simplified into a $F = 0$ ground state and an $F' = 1$ exited state. Furthermore, the 2D problem is treated as quasi-2D by assuming the forces in the two transverse directions are independent and can be summed.

The flux originating from a Knudsen cell at an atomic density $n(T_s)$ with a circular aperture of radius r is given by [22]

$$\Phi_{\text{tot}} = \tfrac{1}{4} n(T_s)\pi r^2 \langle v \rangle, \tag{1}$$

with $\langle v \rangle = \sqrt{8k_B T_s/\pi m}$ the average velocity for a gas in thermal equilibrium in the Knudsen cell at temperature T_s, k_B Boltzmann's constant, and m the mass of the atom. For alkali-metal vapors above the melting temperature, the atomic density can be approximated by [23]

$$n(T_s) = \frac{p^* \exp(-T^*/T_s)}{k_B T_s}, \tag{2}$$

with p^* and T^* constants for the specific atomic element as given in Table I.

Skimming the Knudsen cell by using an aperture with radius r at a distance L_s provides a flux through this aperture of

$$\Phi_{\text{skimmed}} = \Phi_{\text{tot}}\theta^2, \tag{3}$$

with $\theta = r/L_s \ll 1$ the opening angle. Because the brightness is a figure of merit describing ion, not atomic, beams, we assume the atomic beam can be ionized with a 100% efficiency, resulting in a current of

$$I = e\Phi_{\text{skimmed}}, \tag{4}$$

with e the electron charge. From the current and transverse temperature of the thermal source, the transverse reduced brightness of an ion beam with the same properties as the initial atomic beam can now be calculated using the brightness of a thermal emitter [24]:

$$B_r^i = \frac{eJ}{\pi k_B T_t} = \frac{e^2\Phi_{\text{tot}}}{\pi^2 r^2 k_B T_s}, \tag{5}$$

where $J = I/\pi r^2$ the current density and $T_t = T_s\theta^2$ the effective transverse temperature of the atoms leaving the skimmed Knudsen cell.

Filling in the temperature from Tables II, which will be explained further on, results in a brightness of 1.3×10^3 A/(m^2 sr eV) which is four orders of magnitude lower than desired. Laser cooling can decrease the transverse temperature of the atoms to the Doppler temperature [25], increasing the brightness by a factor $T_s\theta^2/T_D$. Using the opening angle from Table II results in a factor 10^2 increase and a brightness of 1.5×10^4 A/(m^2 sr eV) which is still insufficient for use in a FIB.

TABLE II. Parameters given by the analytical model. The top part lists the chosen parameters, the middle part the constraints, and the bottom the results.

Parameter (unit)	Symbol	Value
Source temperature (K)	T_s	383
Cooling and compression length (m)	L_c	0.05
Saturation parameter (−)	s_0	0.67
Detuning (Γ)	δ	−0.5
Initial aperture radius (mm)	r	0.21
Opening angle (mrad)	θ	7.7
Skimmer position or tube length (mm)	L_s	27.3
Magnetic gradient (T/m)	∇B	1.0
Brightness (A/m^{2}depht0pt sr eV)	B_r	7.3×10^7
Flux (s^{-1})	Φ_{skimmed}	7.0×10^9
Knudsen-length number (−)	K_{n,L_s}	2.0

Freinkmans idea [8] for a laser-cooled FIB can be improved by applying compression to the beam using a magnetic field gradient and $\sigma^+ - \sigma^-$ polarized laser beams. Assuming equilibrium has been reached once the spring and kinetic energy of the particles are equal, $k_B T_D = r_f^2 \kappa$ with κ the spring constant, the atomic beam can be compressed to an area of $A_f = \pi r_f^2 = \pi k_B T_D / \kappa$.

With the Doppler temperature and spring constant given by [25]

$$T_D = -\frac{\hbar\Gamma}{8k_B}\frac{\Gamma}{\delta}[1 + s_0 + (2\delta/\Gamma)^2], \tag{6}$$

$$\kappa = -\frac{16\pi\mu_B \nabla B s_0}{\lambda}\frac{\delta/\Gamma}{[1 + s_0 + (2\delta/\Gamma)^2]^2}, \tag{7}$$

with $\hbar$ the reduced Planck constant and μ_B the Bohr magneton, the final brightness of the compressed beam now reads

$$B_r^f = B_r^i \frac{T_s\theta^2}{T_D}\frac{\pi r^2}{Af} = B_r^i \frac{T_s\theta^2}{T_D}\frac{r^2\kappa}{k_B T_D}$$
$$\propto n(T_s) r^2\theta^2 \frac{\nabla B \delta^3 s_0}{[1 + s_0 + (2\delta/\Gamma)^2]^4}. \tag{8}$$

This result shows that the detuning and saturation parameters have an optimum at $\delta = -\Gamma/2$ and $s_0 = I/I_{\text{sat}} = 2/3$, but increasing the source radius r, the source opening angle θ or the magnetic field gradient ∇B will result in unbounded growth of the brightness. This is due to the assumption that all particles coming from the Knudsen cell within the angle θ can be cooled and compressed, which is only true for an infinitely long MOC.

The following part describes how the brightness for a MOC with finite length can be found by placing limits on r, θ, and ∇B. The limit on r is based on the finite displacement an atom experiences by the magneto-optical force during the average interaction time $t = L_c/\langle v\rangle$. The limits on θ and ∇B are based on the assumption that atoms can only be cooled and compressed if their velocities are smaller than the capture velocity and their positions are within the capture radius.

Because the magneto-optical compression force is finite, as is the transfer time trough the MOC, atoms can only be displaced by a finite transverse distance. The actual MOC force (Eq. (7.2) from Ref. [21]) is modeled by maximum acceleration towards the axis for half of the time and maximum deceleration to zero velocity the other half of the time:

$$F_{\text{model}} = F_{MOC,\max} \times \begin{cases} -1, & z < L_c/2, \\ +1, & z \geqslant L_c/2, \end{cases} \tag{9}$$

with $F_{MOC,\max} = F_{MOC}(x = x_c, v_x = 0)$ in which x_c is the capture range. The equations of motion can now be integrated and with an initial velocity of $v_{x,0} = 0$ lead to a maximum displacement of

$$\Delta r_{\max} = \frac{F_{MOC,\max}}{4m}\frac{{L_c}^2}{\langle v\rangle^2}. \tag{10}$$

The initial aperture radius is now set to this maximum displacement: $r = \Delta r_{\max}$.

Cooling and compression is only efficient when the force on the atom is in the linear regime: $F_{MOC} \approx -\kappa x + \alpha v_x$, which holds for particles with a transverse velocity lower than the capture velocity v_c and a position smaller than the capture range x_c. The capture velocity is typically $v_c = \lambda\Gamma/4\pi$ which means that in the paraxial approach the opening angle should be constrained by $\theta = v_c/\langle v\rangle = \lambda\Gamma/(4\pi\langle v\rangle)$. The magnetic field gradient is constrained by setting the capture range equal to the aperture size $r = x_c = \hbar\Gamma/(2\mu_B\nabla B)$, resulting in $\nabla B = \hbar\Gamma/(2\mu_B r)$. The values of these constraints are calculated and listed in Table II. Using these values, the compression increases the brightness by a factor 5×10^2 to 7.3×10^7 A/(m^2 sr eV) [as calculated with Eq. (8)] which is more than an order of magnitude higher than that of the LMIS. The flux [as calculated with Eq. (3)] is larger than the desired value of 6.2×10^9 s^{-1} (1 nA).

The last free parameter to be discussed is the source temperature T_s on which the brightness is exponentially dependent and can thus be used to make a substantial improvement. This parameter is however also bound to a maximum value since Eqs. (3) and (5) are only valid if no interatomic collisions occur between the Knudsen cell and the skimming aperture. An increase in temperature leads to a higher pressure resulting in a shorter mean free path λ_{mfp} and thus to more interatomic collisions in the space between the Knudsen cell and the skimming aperture. The Knudsen number [22] describes the importance of collisions by the ratio between the mean free path and relevant dimension x:

$$K_{n,x} = \frac{\lambda_{mfp}}{x} = \frac{1}{x}(4\sqrt{2}\pi {r_{vdw}}^2 n(T_s))^{-1}, \tag{11}$$

where r_{vdw} is the van der Waals radius of the atom as given by Table I. A Knudsen number higher than unity indicates that the interatomic collisions can be neglected. For the analytical model to be valid, the Knudsen number related to the distance between the Knudsen cell and the skimming aperture $L_s = r/\theta$ is thus required to be higher than 1. The results in Table II shows that this is indeed the case for the chosen temperature.

III. SIMULATIONS

In the previous section an analytical model was introduced that allows us to make initial predictions about the brightness that can be expected from a compact MOC. The

model is, however, a simplification of the actual cooling and compression mechanism and may not yield realistic results for the performance of the actual system including the atomic structure of rubidium and the collimating tube. Doppler cooling simulations allow for a more accurate description of the laser-cooling and compression process and thus better predictions for the MOC performance. In this section the simulations are verified against the analytical model after which the simulations are expanded to include the effects of the real atomic structure of rubidium and the distributions that can be expected from a real thermal source. Finally, a set of parameters is found which allows the MOC to achieve the desired brightness and current within only a few centimeters.

The simulation software [26] traces atoms trough a light field while taking the effect of each absorption-emission cycle into account. Mind that the atoms do not interact with each other and thus no collisions are taken into account. In order to allow for quasi-2D results, pairs of half-atoms are traced trough a 1D light and magnetic field. The half-atoms in such a pair have identical longitudinal velocity but different transverse positions and velocities and thus represent the x and y coordinates of one full atom. In the post-processing these half-atoms are combined and the brightness and flux figures can be calculated for collections of these atoms. Instead of using Eq. (5) for calculating the brightness the reduced version of Eqs. (1) and (2) from Ref. [27] are used because these equations are also valid for beams with correlations and non-Gaussian beam shapes. Depending on the parameters, 10^5 to 10^7 atoms need to be traced in order to have good statistics. The code has also undergone modifications to include the starting distributions for both a skimmed and a collimated Knudsen cell. These distributions were found by a geometrical calculation and Monte Carlo simulations under the assumption that the atoms only interact with the wall of the collimation tube (thus $K_n \gg 1$).

Before using the simulations for scenarios surpassing the analytical model, it is checked against this model. Then the effects of including the actual level structure of rubidium are investigated, followed by the collimation tube on the Knudsen cell. Finally, the parameters are varied to find the optimal performance of the MOC.

A. Verification

The simulation is checked against the analytical model by looking at the scaling of the brightness with the laser detuning. In order to do so, a hypothetical atom is assumed which has all the physical properties of the ^{85}Rb isotope except for the ground state having the total angular momentum quantum number $F = 0$ and the excited state $F' = 1$. This is done to mimic the two-level atom that is used in the analytical model. For the thermal source the atom longitudinal velocity is taken equal to the average velocity, the position is uniformly distributed over a circle with radius r, and the angle uniformly distributed between θ and $-\theta$. In the following analysis the brightness of the 10% fraction of the atoms which are closest to the axis at the end of the MOC is reported because this provides a good indication of the center brightness.

Figure 2 shows the comparison between the analytical model and simulations of a MOC with a length between 5 cm and 1 m. As predicted by the analytical model, the brightness has a maximum for a detuning around $-\Gamma/2$. However, the brightness at a length of 5 cm is two orders of magnitude lower than the analytical model predicts. At 1 m the simulation matches the analytical result, indicating that eventually the Doppler temperature and equipartition of kinetic and potential energy in the transverse direction is reached.

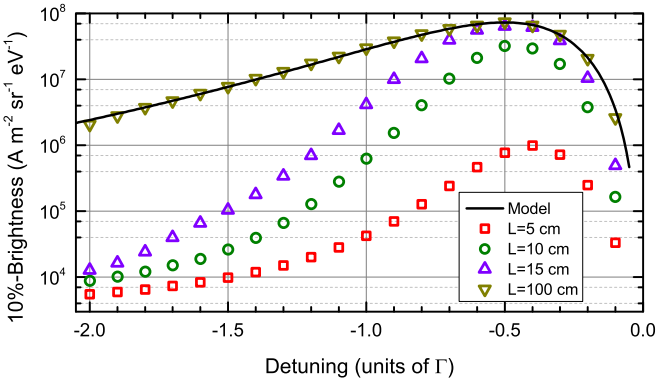

FIG. 2. (Color online) 10% brightness $B_r^{10\%}$ plotted on a logarithmic scale as a function of the detuning, for different cooling and compression stage lengths L. As L increases, the beam is cooled and compressed more into equilibrium and the simulation results (scattered) converge to the analytical results (solid line). The parameters used are given in Table II.

The difference between the model and the simulations is explained by an overestimation of the average magneto-optical force in Eq. (9). Figure 3 shows the trajectories calculated by the numerical integration of the equations of motion for the model force [Eq. (9)] and the actual magneto-optical force (Eq. (7.2) in Ref. [21]) for the parameters in Table II. This indicates that it takes the atom more than twice the distance to get compressed into r_f than expected from the model. For particles at the same starting position and a positive initial v_x

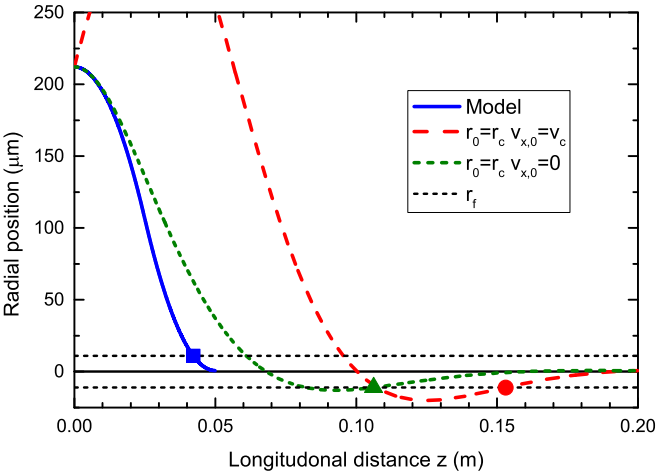

FIG. 3. (Color online) Trajectories of particles in a MOC with parameters given by Table II with $v_z = \langle v \rangle = 309$ m/s and different starting conditions as a result of the actual MOC force from Ref. [21] (dashed lines) and the model force of Eq. (9). Indicated are the distances after which the particle radial position stays smaller than the final radius r_f.

TABLE III. Performance of different rubidium isotopes.

Isotope	10% brightness A/(m^2 sr eV)	10% flux s^{-1}
Two-level Rb	7.8×10^5	7.1×10^8
Isotopically pure ^{85}Rb	1.5×10^5	7.1×10^8
Isotopically pure ^{87}Rb	4.6×10^5	7.1×10^8
^{85}Rb in natural abundance	1.1×10^5	5.1×10^8
^{87}Rb in natural abundance	1.3×10^5	2.0×10^8

this is even larger, explaining why for a detuning of $-\Gamma/2$ a MOC length of around 15 cm is required to reach the brightness value as predicted by the analytical model. For larger detunings, the capture range, and thus the position at which the force is maximum, is larger. Particles on the edge of the aperture now experience a smaller force than the maximum and thus the displacement the atom will experience is lower than that given by Eq. (10). This requires an even longer MOC for achieving the predicted brightness.

Now that the difference between the analytical model and the simulations is explained, a more accurate description of the rubidium atomic structure and the thermal source can be implemented in the simulations in order to predict the performance of the actual system.

B. Real rubidium

In the following analysis, simulations are performed using the real atomic structure of the ^{85}Rb and ^{87}Rb isotope with the $F = 3$ to $F' = 4$ ($F = 2$ to $F' = 3$) cooling transitions. We only included the cooling transition and thus assume an ideal repumper is present which brings all atoms to the correct ground state and keeps them there. Table III summarizes the differences in peak brightness and flux for the different isotopes of rubidium for the parameters in Table II.

As a general rule, laser cooling becomes less efficient with more magnetic sublevels. This explains why the two-level rubidium performs better than the real isotopes and why ^{87}Rb performs better than the lighter isotope. Although isotopically pure ^{87}Rb gives the best performance, our source will use ^{85}Rb in the natural abundance as this is inexpensive. Using the parameters as provided by the analytical model, both the target brightness and flux cannot be reached and thus optimization is required.

C. Collimated tube source

In order to increase the brightness and flux of the source, a Knudsen cell with a collimation tube could be used instead of the skimmer as was used in the models. The collimation tube increases the flux density at the MOC entrance and also increases the lifetime of the source. For a heated tube with opening angle $\theta = r/L_s$ the flux is given by [16]

$$\Phi_{\text{tube}} = \Phi_{\text{tot}} 8/3 \times \theta \, (1 + 8/3 \times \theta)^{-1} . \tag{12}$$

For small opening angles $\theta \ll 1$ this flux is a factor $3/(8\theta)$ higher than that of the skimmed Knudsen cell that is given by Eq. (3). Furthermore, in the skimmed source, the flux leaving the Knudsen cell is given by Eq. (1) but only the flux as described by Eq. (3) leaves the second aperture; the difference

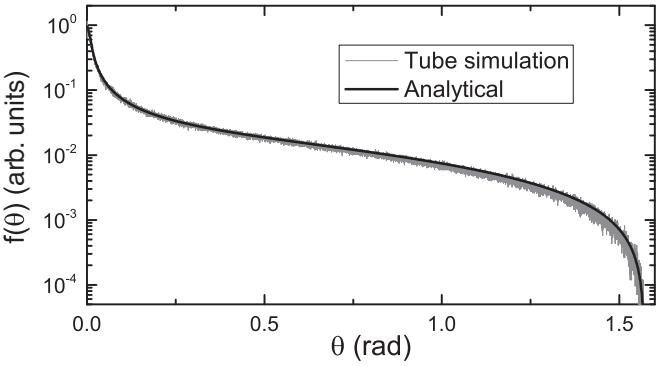

FIG. 4. Angular distribution $f(\theta)$ of particles coming from a collimating tube with the dimensions given in Table II. In grey the results of the Monte Carlo simulation are given; in black is the analytical prediction as given by Eqs. (8) and (9) from Ref. [16].

is lost into the vacuum. The collimating tube reflects a large fraction of the flux back into the Knudsen cell, reducing the loss of atoms thus increasing the lifetime of the source, which is given by

$$t_{\text{life}} = \frac{N_A M}{m \Phi} \tag{13}$$

in which M is the total mass of rubidium in the source, m the mass of a single rubidium atom, and N_A is Avogadro's number. For our set of parameters the lifetime of the skimmed source including 100 mg of rubidium is only 70 days whereas the collimated Knudsen cell lasts for 10 years. Furthermore, the flux from this source is increased by a factor 341.

The increase in flux is impressive, but the transverse velocity distribution from the collimating tube is also much broader, resulting in a lower fraction of particles that can be captured by the MOC. To see the influence of these two competing processes, simulations were performed using the actual particle distributions for a collimating tube. The tube was implemented in the software by tracing the particles trough the tube assuming inelastic collisions with the walls following a cosine-distribution. This implementation was verified by comparison with the theoretical prediction [Eqs. (8) and (9) from Ref. [16]) as is shown in Fig. 4.

The analysis on the laser cooling simulations with the collimating tube is performed on a brightness-flux profile (Fig. 5) instead of the 10%-brightness number as was done before. Such a profile is constructed by selecting the beam after the MOC by means of an aperture and calculating the brightness and flux of the remaining atoms. Increasing the aperture size will lead to more flux being selected and a different brightness. The flux and brightness for different aperture sizes are plotted in a single graph on the x and y axes respectively.

Figure 5 shows how the brightness-flux profile of the skimmed and the collimated source compare for the parameters from Table II. First, observe the much larger flux coming from the collimating tube. Then, also note the higher center brightness of the cooled and compressed beam. We credit this effect to the higher flux density in the tube. For a FIB, only the center 1 nA of current, corresponding to a flux of 6.2×10^9 s^{-1}, is of importance, therefore we will now report

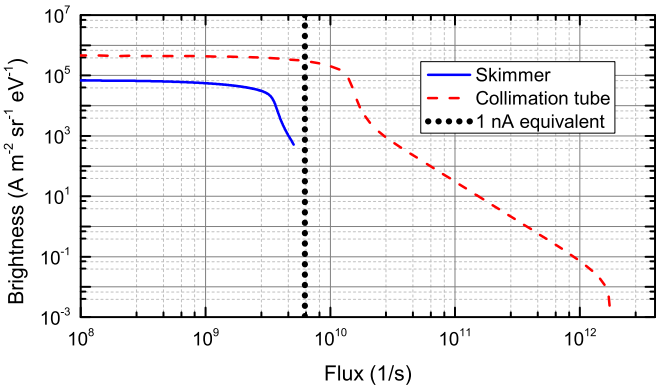

FIG. 5. (Color online) Brightness-flux plot for a skimmed and a collimated Knudsen cell with the aperture/tube radius and opening angle given by Table II. For the collimated source, both the peak brightness and the total flux are higher.

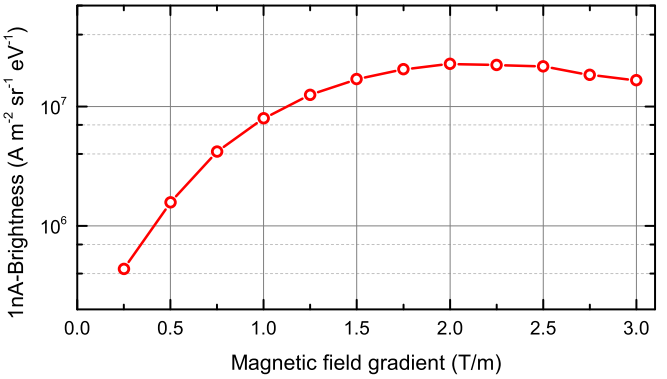

FIG. 7. (Color online) Brightness for different magnetic field gradients. The other parameters can be found in Table II except for $r = 1.0$ mm and $\theta = 36$ mrad. Maximum brightness is achieved at $\nabla B = 2.0$ T/m.

on the brightness of this part of the beam. Using the collimation tube, a brightness of 3.0×10^5 A/(m^2 sr eV) at the target flux can be achieved which is still a factor 3.3 short of the target brightness.

D. Optimization

So far, the parameters found by the analytical model, as given in Table II, are used to predict the performance of the system. Here, the brightness for a flux of 6.2×10^9 s^{-1} (1 nA) is optimized by variation of these parameters.

For the total flux scales with the third power of the collimation tube radius r, this is the first parameter to be considered. Introducing more atoms to the MOC will result in more particles being cooled and compressed and thus a higher brightness. Figure 6 shows the results of simulations using different tube radii, where the length of the tube has been kept constant. Increasing the tube radius does indeed result in a higher brightness (red circles), but the increase in brightness is less than what would be expected if all additional particles could be laser cooled (blue squares). This is caused by the fact that not all the atoms at large radial position can be compressed. The increase in tube radius, and thus the flux, also decreases the source lifetime, creating a tradeoff between the lifetime and the brightness. Here, we chose to take the tube radius $r = 1.0$ mm as this yields a brightness 10 times higher than the target value. It decreases the lifetime only by a factor 100 to 1 year for 1 gram of rubidium in the natural mixture.

In the analytical model, the magnetic field gradient was chosen such that all particles could be compressed. Increasing this field results in fewer particles being captured but also a larger spring constant and thus a higher beam density. Simulations were performed to check at which scale of the magnetic field gradient this tradeoff is important. As is shown in Fig. 7 an optimum indeed exists at a gradient strength of 2.0 T/m which improves the brightness by a factor 2.3.

The final parameter to check is the MOC length L_c. Figure 8 shows that the compact 5 cm long MOC performs well: making it twice as short decreases the brightness by a factor 7 whereas making it twice as long increases the brightness only by a factor 2.5. A longer MOC requires lager beam aspect ratios or higher laser power and custom optics so 5 cm also seems a practical length.

At 5 cm the brightness at 1 nA reads 2.1×10^7 A/(m^2 sr eV) which is more than a factor 10 higher than the target. From the particle distributions at the end of the MOC the flux density

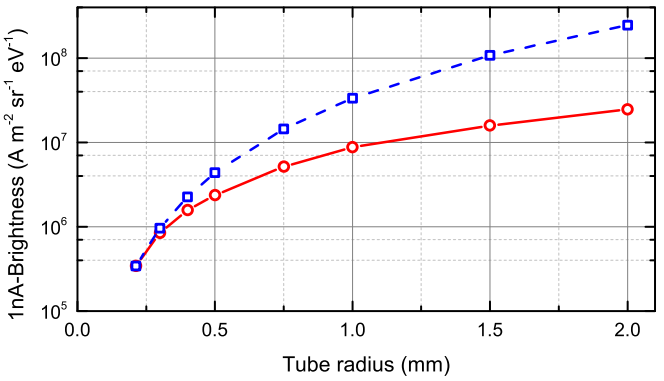

FIG. 6. (Color online) The brightness (red circles) for collimation tubes with different radii but equal length. The blue squares indicate how the brightness would increase if all the additional flux could be cooled and compressed.

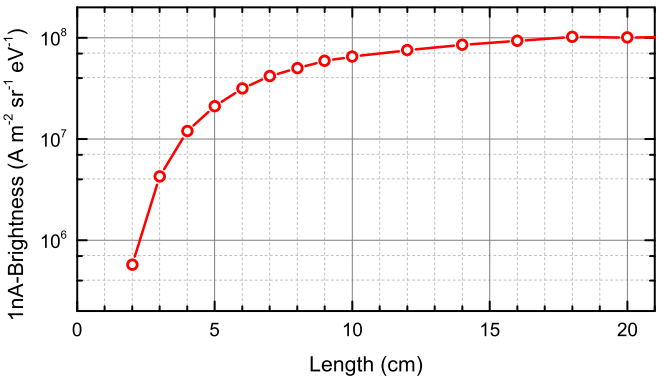

FIG. 8. (Color online) Brightness for different MOC lengths. The other parameters can be found in Table II except for $r = 1.0$ mm, $\theta = 36$ mrad and $\nabla B = 2.0$ T/m. Increasing the MOC length does improve the brightness but not to a great extent.

was calculated to be 4×10^{19} m^{-2} s^{-1} whereas a transverse temperature of 2 mK was found. Note that this temperature is significantly higher than the Doppler limit which is caused by the two-level atom picture breaking down for ^{85}Rb in a $\sigma^+ - \sigma^-$ polarized light field due to the many magnetic sublevels.

The performance may be improved even further by increasing the saturation parameter or source temperature. Although increasing the saturation parameter raises the Doppler temperature, it also leads to more particles being captured. As the simulation program does not include cross-saturation effects like stimulated emission by the opposite laser beam, the high saturation parameter regime was not investigated. The same holds for the higher source temperature: an increase leads to more interparticle collisions in the collimation tube, making the transverse velocity distribution broader than that of the collision-free model that is used in the simulations. We expect the effect of this broadening to be less important than the increase in flux from the higher temperature. The brightness therefore still increases, but less than what would be expected from the higher flux.

IV. TOWARDS AN ACTUAL FIB

This work has shown that a high-brightness atomic beam can be formed in a compact MOC. In order to make use of this beam in an actual FIB, the atoms should be transported and ionized while conserving the brightness. This section describes which requirements must be met to achieve this goal.

In a practical apparatus the beam selection and ionization have to take place some distance from the MOC. Because the atomic beam is far from monochromatic, the transverse reduced brightness is not a conserved quantity and thus will decrease with the distance from the MOC. Numerical calculation shows that, when placing the beam-defining aperture at 5 mm from the MOC, the brightness still reads half of the starting value. Ionization thus has to take place within a few mm from the MOC.

A high degree of ionization is required to create an ion beam with the same density and thus brightness of the atomic beam. Ionization is performed using a saturated ($s_0 \gg 1$) excitation beam at 780 nm and an ionization beam at 480 nm. A simple rate equation model is used to estimate the required intensity of the ionization laser. Assuming an excited state population of 1/2 and a uniform ionization laser intensity I_i starting at $z = 0$, the rate of ionization is given by $R_i = \lambda_i \sigma_i I_i/(4\pi c\hbar)$ were the constants can be found in Table I. Integration results in a fraction of ionized atoms of

$$F(z) = 1 - \exp\left(\frac{\lambda_i \sigma_i}{4\pi c\hbar \langle v\rangle} I_i\, z\right). \tag{14}$$

In order to ionize 95% of the atoms within 3 μm an ionization intensity of 5×10^{11} W/m^2 is required which can be achieved using a build-up cavity and a commercially available laser of several tens of mW. Preliminary calculations using the optical Bloch equations and Gaussian shaped laser beams confirm this simple estimation.

After the ionization has taken place, the ions need to be accelerated in order to reduce the Coulomb interactions between them. Increasing the extraction field E will reduce the heating caused by these interactions but will also introduce longitudinal energy spread which lowers the achievable resolution of the FIB due to chromatic aberrations in the lens column. Reference [28] discusses this problem in detail and shows that, using the brightness as reported in this work, a subnanometer spot size can be achieved at a current of 1 pA.

V. CONCLUSION

In this paper we have discussed the possibility of creating a high-quality atomic beam of rubidium as a precursor for a high-brightness ionic beam for use in a FIB. First, the proposed setup consisting of a collimated Knudsen cell and a 2D MOC was introduced. An analytical model was set up to predict the performance of the system and to gain insight in the relevant parameters. This model was used to verify Monte Carlo simulations on the laser cooling process. The simulation program was extended to include the atomic structure of the ^{85}Rb and ^{87}Rb isotopes and the initial position and velocity distributions of atoms originating from a collimated tube source. Optimization of the relevant parameters lead to a predicted atomic beam brightness of 2.1×10^7 A/(m^2 sr eV) at a flux of 6.2×10^9 s^{-1} (equivalent to a current of 1 nA). By efficient photoionization as close as possible to the MOC this can result in an ion beam brightness higher than that of the LMIS. Furthermore a substantial ion beam current of 1 nA can be realized.

ACKNOWLEDGMENTS

This research is supported by the Dutch Technologiestichting STW, applied science division of the "Nederlandse Organisatie voor Wetenschappelijk Onderzoek (NWO)", FEI Company, Pulsar Physics and Coherent Inc..

[1] V. Raffa, P. P. Castrataro, A. Menciassi, and P. Dario, in *Applied Scanning Probe Methods II - Scanning Probe Microscopy Techniques* (Springer, Berlin, 2006).
[2] J. Orloff, Rev. Sci. Instrum. **64**, 1105 (1993).
[3] C. W. Hagen, E. Fokkema, and P. Kruit, J. Vac. Sci. Technol. B **26**, 2091 (2008).
[4] B. W. Ward, J. A. Notte, and N. P. Economou, J. Vac. Sci. Technol. B **24**, 2871 (2006).
[5] R. H. Livengood, S. Tan, R. Hallstein, J. Notte, S. McVey, and F. Faridur Rahman, Nucl. Instrum. Methods Phys. Res., Sect. A **645**, 136 (2011).
[6] S. Tan, R. Livengood, D. Shima, J. A. Notte, and S. McVey, J. Vac. Sci. Technol. B **28**, C6F15 (2010).
[7] D. Jun, V. Kutchoukov, C. Heerkens, and P. Kruit, Microelectron. Eng. **97**, 134 (2012).
[8] B. G. Freinkman, A. V. Eletskii, and S. I. Zaitsev, Microelectron. Eng. **73-74**, 139 (2004).
[9] S. B. van der Geer, M. P. Reijnders, M. J. de Loos, E. J. D. Vredenbregt, P. H. A. Mutsaers, and O. J. Luiten, J. Appl. Phys. **102**, 094312 (2007).
[10] B. Knuffman, A. V. Steele, J. Orloff, and J. J. McClelland, New J. Phys. **13**, 103035 (2011).

[11] M. P. Reijnders, P. A. van Kruisbergen, G. Taban, S. B. van der Geer, P. H. A. Mutsaers, E. J. D. Vredenbregt, and O. J. Luiten, Phys. Rev. Lett. **102**, 034802 (2009).

[12] N. Debernardi, R. W. L. van Vliembergen, W. J. Engelen, K. H. M. Hermans, M. P. Reijnders, S. B. van der Geer, P. H. a. Mutsaers, O. J. Luiten, and E. J. D. Vredenbregt, New J. Phys. **14**, 083011 (2012).

[13] Z. T. Lu, K. L. Corwin, M. J. Renn, M. H. Anderson, E. A. Cornell, and C. E. Wieman, Phys. Rev. Lett. **77**, 3331 (1996).

[14] B. Knuffman, A. V. Steele, and J. J. McClelland, J. Appl. Phys. **114**, 44303 (2013).

[15] L. Kime, A. Fioretti, Y. Bruneau, N. Porfido, F. Fuso, M. Viteau, G. Khalili, N. Santic, A. Gloter, B. Rasser, P. Sudraud, P. Pillet, and D. Comparat, Phys. Rev. A **88**, 033424 (2013).

[16] D. R. Olander and V. Kruger, J. Appl. Phys. **41**, 2769 (1970).

[17] S. C. Bell, M. Junker, M. Jasperse, L. D. Turner, Y.-J. Lin, I. B. Spielman, and R. E. Scholten, Rev. Sci. Instrum. **81**, 013105 (2010).

[18] D. A. Steck, "Rubidium 85 and 87 D Line Data", available online at http://steck.us/alkalidata/

[19] M. Matina, in *Handbook of Chemistry and Physics*, 94th ed., edited by W. M. Haynes (CRC Press, Boca Raton, FL, 2013-2014).

[20] C. Gabbanini, S. Gozzini, and A. Lucchesini, Opt. Commun. **141**, 25 (1997).

[21] H. J. Metcalf and P. van der Straten, *Laser Cooling and Trapping* (Springer, Berlin, 1999).

[22] H. Pauly, in *Atomic and Molecular Beam Methods*, Vol. 1, edited by G. Scoles (Oxford University Press, Oxford, 1988), p. 84.

[23] C. B. Alcock, in *Handbook of Chemistry and Physics*, 94th ed., edited by W. M. Haynes (CRC Press, Boca Raton, FL, 2013-2014).

[24] O. J. Luiten, B. J. Claessens, S. B. van der Geer, M. P. Reijnders, G. Taban, and E. J. D. Vredenbregt, Int. J. Mod. Phys. A **22**, 3882 (2007).

[25] C. J. Foot, *Atomic Physics* (Oxford University Press, Oxford, 2005).

[26] E. J. D. Vredenbregt and K. A. H. van Leeuwen, Am. J. Phys. **71**, 760 (2003).

[27] B. J. Claessens, S. B. van der Geer, E. J. D. Vredenbregt, and O. J. Luiten, Phys. Rev. Lett. **95**, 164801 (2005).

[28] G. ten Haaf, S. H. W. Wouters, S. B. van der Geer, E. J. D. Vredenbregt, and P. H. A. Mutsaers, arXiv:1410.4362.